ELSEVIER

Materials Science and Engineering A 449–451 (2007) 1049–1051

MATERIALS SCIENCE & ENGINEERING A

www.elsevier.com/locate/msea

Influence of La on the crystallisation behaviour of amorphous $Al_{94-x}Ni_6La_x$ ($x = 4$–7) alloys

M. Wollgarten [a,*], K.L. Sahoo [b], J. Haug [a], J. Banhart [a]

[a] *Hahn-Meitner Institute, Materials Department SF 3, Glienicker Str. 100, D-14109 Berlin, Germany*
[b] *National Metallurgical Laboratory, Jamshedpur 831007, India*

Received 21 August 2005; received in revised form 4 January 2006; accepted 28 February 2006

Abstract

Melt spun and subsequently annealed Al-alloys with 6 at.% Ni and 4–7 at.% La were investigated by differential scanning calorimetry, X-ray diffractometry (XRD). XRD reveals that the ribbons are fully amorphous in the as melt spun state. DSC shows that crystallisation proceeds in two stages which are sensitively influenced by the La content. The first stage compromises the formation of either fcc-Al (at low La content) or a bcc phase (at high La concentration) of yet unknown composition. Micro hardness changes significantly during annealing and can be correlated to the different stages of microstructural transformation as observed by XRD.

Keywords: Amorphous Al-alloys; Crystallisation; Scattering methods

1. Introduction

Amorphous and nanocrystalline Al–TM–RE alloys (TM = transition metal, RE = rare-earth elements or Y), particularly in Al–Ni–RE alloys show promising mechanical properties which are superior to that of normal crystalline high-strength Al-alloys [1,2]. Various Al–TM–RE alloys are well investigated with regard to formation and stability of the amorphous phase and crystallisation pathways upon annealing (see e.g. [1,3–5]). Insufficient knowledge exists for Al–TM–La system. Here, we report on the crystallisation pathways and the evolution of hardness of amorphous Al–Ni–La alloys.

Besides the experiments reported here, $Al_{94-x}Ni_6La_x$ alloys have been studied by small angle neutron scattering [6]. Those measurements support the view that the La content has significant influence both on the initial microstructure (see hardness and crystallisation onset) and crystallisation pathways.

2. Experimental methods

Ribbons of compositions $Al_{94-x}Ni_6La_x$ ($x = 4$–7, designated La4 to La7) were prepared by melt spinning at a wheel speed of 40 m/s. Further details of the preparation process can be found in Ref. [6]. The ribbons were found to be fully amorphous in X-ray diffraction (XRD) measurements and were further studied by differential scanning calorimetry (DSC) under argon atmosphere. Isochronal studies were done at heating rates ranging from 5 to 40 K/min. A second scan at the same rate was used for obtaining the base line. Isothermal experiments were conducted by heating the ribbons to the desired temperature at 100 K/min followed by a dwell period of up to 20 min and rapid cooling to room temperature. The annealed samples were studied by XRD, too.

Energy filtered transmission electron microscopy (EFTEM) was used to study the La distribution in annealed samples.

Evolution of hardness with temperature was studied by annealing as melt spun ribbons for 10 min at various temperatures between room temperature and 480 °C followed by a Vickers-type hardness measurement.

Determination of the full width at half maximum of the Al ⟨1 1 1⟩, Al_3Ni ⟨1 1 1⟩ and $Al_{11}La_3$ ⟨1 0 3⟩ XRD maxima was used to estimate the mean particle sizes [7].

3. Results and discussion

The as melt spun material was found to be amorphous in XRD. Upon continuous heating in DSC each alloy shows two distinct crystallisation events. The peak temperatures (T_{P_1}) of

* Corresponding author.
E-mail address: wollgarten@hmi.de (M. Wollgarten).

0921-5093/$ – see front matter © 2006 Published by Elsevier B.V.
doi:10.1016/j.msea.2006.02.351

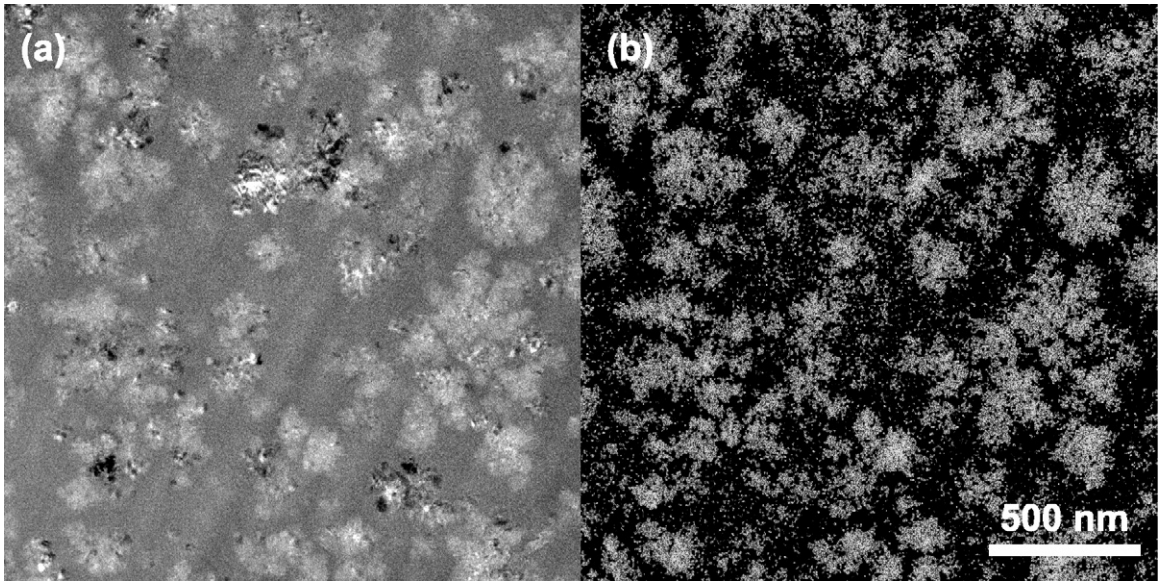

Fig. 1. (a) Bright field image obtained by energy filtered transmission electron microscopy (EFTEM) of a melt spun $Al_{87}Ni_6La_7$ alloy annealed at 230 °C for 2 h (zero loss image). (b) La distribution map of the same area derived from three EFTEM images around the La-M edge (three window method).

the first event range between 215 °C (La7) and 233 °C (La4). The respective values of the second crystallisation fall between 334 °C (La4) and 317 °C (La7). Our results are in accordance with the respective data found in the literature for other Al–Ni–La alloys [1,3,6,8–10]. The overall tendency is that T_{P_1} increases while T_{P_2} is lowered with increasing amount of La and Ni, respectively.

The crystallisation products of the first event were identified by XRD as fcc-Al (in La4, La5, La6) and a second phase (in La6, La7). The latter compound could not be identified by a known binary or ternary compound of Al, Ni and La. Quantitative analysis of the diffraction showed that it has bcc structure with a lattice constant of 0.663 nm. The products of the second crystallisation were determined as $Al_{11}La_3$ and Al_3Ni (in La4 to La6). In La7, the metastable phase that formed during the first crystallisation stage decomposes into fcc-Al and $Al_{11}La_3$.

The crystallisation pathways reported here for the Al–Ni–La system are exceptional among all known Al–Ni–RE alloys, where generally fcc-Al is the only primary crystallisation product. In contrast, we find that a bcc phase precipitates if the La concentration exceeds 6 at.%. The extremely low solid solubility of La in Al (0.01 at.% at 640 °C [11]) cannot be regarded as explanation for the observation as other rare earth elements, e.g. Ce, show a similar solubility [11]. However, La is the largest atom of all rare earth elements. This might point to kinetic constraints governing phase formation in amorphous Al–Ni–La alloys. Increasing La content may block crystallisation of pure fcc-Al, since the atomic radius of La (0.188 nm) is significantly larger than that of Al (0.143 nm) which makes La diffusion difficult. This argument is supported by an increase of activation energy [6] of the first crystallisation stage with increasing La content up to 6 at.%. At about 6 at.% La crystallisation of a bcc type phase becomes more favourable.

This phase takes the excess amount of La which is demonstrated by the La distribution map obtained by EFTEM (Fig. 1). Ronto et al. [8] observe a similar phenomenon in an amorphous $Al_{87}Ni_7La_6$ alloy and report the formation of a primitive cubic (pc) phase besides simultaneous crystallisation of fcc-Al. It might be worthwhile to study the structural differences to find out whether they can be related to the different Ni-content of the alloys.

Isothermal DSC experiments at temperatures around T_{P_1} and T_{P_2} were used to investigate the crystallisation kinetics. Here, the compositional differences go along with differences in the evolution of heat flow. For La5 we find (within the time resolution of the DSC apparatus) an instant increase of heat flow poiting to a immediate growth of particles. Such an observation is not unusual as it has be reported for amorphous $Al_{87}Ni_{10}Ce_3$ [12], amorphous $Al_{83}Mn_{17}$ films [13] or in amorphous binary Al–La [14,15]. On the other side La6 and La7 show a incubation time before heat flow is observed which is interpreted as a nucleation stage that precedes the subsequent growth of particles.

The differences between the present alloys observed up to here are also visible in their macroscopic behaviour. Fig. 2(a) depicts the evolution of hardness as a function annealing temperature. For La4 and La5, hardness starts to increase at about 100 and 140 °C, respectively, where primary crystallisation sets in. At the onset of the second crystallisation stage a sharp drop is observed. On the other side, the hardness of La6 and La7 ribbons rises slowly up to 290 °C and up to 270 °C, respectively, followed by a fairly abrupt decrease for La6 and a comparatively small decrease for La7.

The differences measured by DSC find their counterpart in these observations. The as melt spun samples differ in hardness: La4 and La5 have a substantial lower hardness than La6 and La7. In addition, the hardness of the former alloys show a much steeper hardness increase, which corresponds to the immediate crystallisation of fcc-Al particles. These particles strengthen the alloy up to the point where the stable phases start to form from

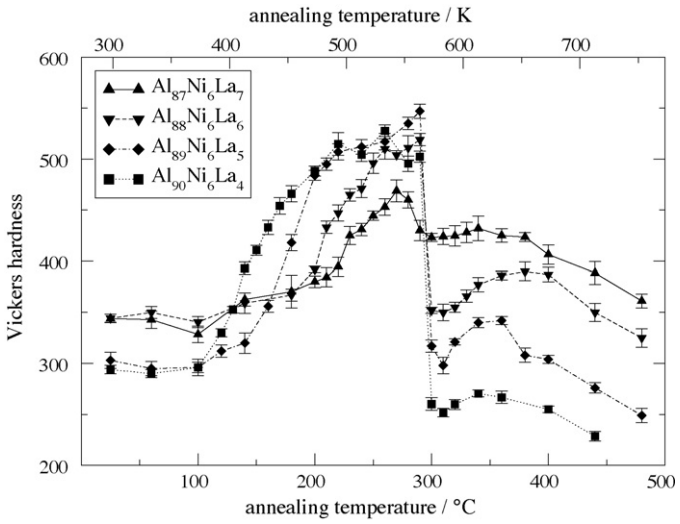

Fig. 2. Evolution of hardness of amorphous $Al_{94-x}Ni_6La_x$ ribbons at 0.2 N load. Each sample was annealed for 10 min at the indicated temperature. Each hardness value is the average of 10 measurements.

the supersaturated matrix. Particle growth has been measured by XRD peak width analysis and supports this interpretation. Growth of fcc-Al particles is very slow up to 290 °C. At higher temperatures (above 290 °C for La5 alloy), substantial growth of Al particles is observed and decomposition of the amorphous matrix results in precipitation of $Al_{11}La_3$ and Al_3Ni. As a consequence hardness decreases significantly.

The differences in the crystallisation pathways are best recognised for La7 around those annealing temperatures which lead to the highest hardness values. The moderate rise of hardness starting at about 100 °C results from the sole formation of the metastable bcc phase instead of fcc-Al as found in La4 to La6. The drop of hardness at about 270 °C is small compared to La4 to La6 due to the crystallisation of fcc-Al which causes the main hardening effect.

In the fully crystallised state the final hardness reflects the La content due to increasing amounts of intermetallic phases in the matrix (Fig. 2).

Acknowledgements

The authors thank C. Aussedat for her help in the hardness measurements and M.-P. Macht for fruitful discussion.

References

[1] A. Inoue, Prog. Mater. Sci. 43 (1998) 365.
[2] Y. He, S.J. Poon, G. Shiflet, Science 241 (1988) 1640.
[3] A.K. Gangopadhyay, K.F. Kelton, Philos. Mag. A 80 (2000) 1193.
[4] O.N. Senkov, J.M. Scott, D.B. Miracle, J. Alloys Compd. 337 (2002) 83.
[5] F. Ye, K. Lu, J. Non-Cryst. Solids 262 (2000) 228.
[6] K.L. Sahoo, M. Wollgarten, J. Haug, J. Banhart, Acta Mater. 53 (2005) 3861.
[7] B.D. Cullity, Elements of X-ray diffraction, Edison Wesley, London, 1978, p. 284.
[8] V. Ronto, L. Battezzati, A.R. Yavari, M. Tonegaru, N. Lupu, G. Heunen, Scripta Mater. 50 (2004) 839.
[9] A. Inoue, K. Ohtera, A.P. Tsai, T. Masumoto, Jpn. J. Appl. Phys. 27 (1988) L280.
[10] K.L. Sahoo, M. Wollgarten, K. B. Kim, J. Banhart, J. Mater. Res. 20 (2005) 2927.
[11] K.A. Gschneider, F.W. Calderwood, in: T.B. Massalski (Ed.), Binary Alloy Phase Diagrams, vol. 1, Metals Park, Ohio, 1986.
[12] A. Inoue, K. Nakazato, Y. Kawamura, A.P. Tsai, T. Masumoto, Mater. Trans. JIM 35 (1994) 95.
[13] L.C. Chen, F. Spaepen, Nature 336 (1988) 366.
[14] B. Dill, Y. Li, M. Al-Khafaji, W.M. Rainforth, R.A. Buckley, H. Jones, J. Mater. Sci. 29 (1994) 3913.
[15] A. Inoue, in: K.A. Gschneider, L. Eyring (Eds.), Handbook on the Physics and Chemistry of Rare Earths, vol. 24, Elsevier, Amsterdam, 1997.